Chemical Synthesis of Novel Plasmonic Nanoparticles

Xianmao Lu,[1] Matthew Rycenga,[1] Sara E. Skrabalak,[2] Benjamin Wiley,[3] and Younan Xia[1]

[1]Department of Biomedical Engineering, Washington University, St. Louis, Missouri 63130; email: xia@biomed.wustl.edu

[2]Department of Chemistry and [3]Department of Chemical Engineering, University of Washington, Seattle, Washington 98195

Annu. Rev. Phys. Chem. 2009. 60:167–92

First published online as a Review in Advance on October 31, 2008

The *Annual Review of Physical Chemistry* is online at physchem.annualreviews.org

This article's doi: 10.1146/annurev.physchem.040808.090434

0066-426X/09/0505-0167$20.00

Key Words

shape-controlled synthesis, noble-metal nanostructures, localized surface plasmon resonance, surface-enhanced Raman scattering, photothermal effect

Abstract

Under the irradiation of light, the free electrons in a plasmonic nanoparticle are driven by the alternating electric field to collectively oscillate at a resonant frequency in a phenomenon known as surface plasmon resonance. Both calculations and measurements have shown that the frequency and amplitude of the resonance are sensitive to particle shape, which determines how the free electrons are polarized and distributed on the surface. As a result, controlling the shape of a plasmonic nanoparticle represents the most powerful means of tailoring and fine-tuning its optical resonance properties. In a solution-phase synthesis, the shape displayed by a nanoparticle is determined by the crystalline structure of the initial seed produced and the interaction of different seed facets with capping agents. Using polyol synthesis as a typical example, we illustrate how oxidative etching and kinetic control can be employed to manipulate the shapes and optical responses of plasmonic nanoparticles made of either Ag or Pd. We conclude by highlighting a few fundamental studies and applications enabled by plasmonic nanoparticles having well-defined and controllable shapes.

INTRODUCTION

Plasmon resonance is an optical phenomenon arising from the collective oscillation of conduction electrons in a metal when the electrons are disturbed from their equilibrium positions (1, 2). Such a disturbance can be induced by an electromagnetic wave (light), in which the free electrons of a metal are driven by the alternating electric field to coherently oscillate at a resonant frequency relative to the lattice of positive ions. For a bulk metal of infinite size, the frequency of oscillation ω_p can be described by $\omega_p = (Ne^2/\varepsilon_0 m_e)^{1/2}$, where N is the number density of conduction electrons, ε_0 is the dielectric constant of vacuum, e is the charge of an electron, and m_e is the effective mass of an electron (1). Thus, the bulk plasmon frequency of a particular metal depends only on its free electron density. The plasmon frequencies for most metals occur in the ultraviolet (UV) region, with alkali metals and some transition metals such as Cu, Ag, and Au exhibiting plasmon frequencies in the visible region.

Because the penetration depth of an electromagnetic wave on a metal surface is limited (<50 nm for Ag and Au), only plasmons caused by surface electrons are significant (3) and are commonly referred to as surface plasmons. If a surface plasmon is associated with an extended metal surface, it is called a propagating surface plasmon. The frequency of a propagating surface plasmon is lower than the bulk frequency, with the theoretical propagating-surface-plasmon frequency corresponding to $\omega_p/\sqrt{2}$ when the boundary conditions of a metal-vacuum interface are applied. **Figure 1*a*** illustrates such a plasmon, which causes alternating positive and negative charges along a metal surface with the propagation of the electron density waves. If the collective oscillation of free electrons is confined to a finite volume as with a metal nanoparticle, the corresponding

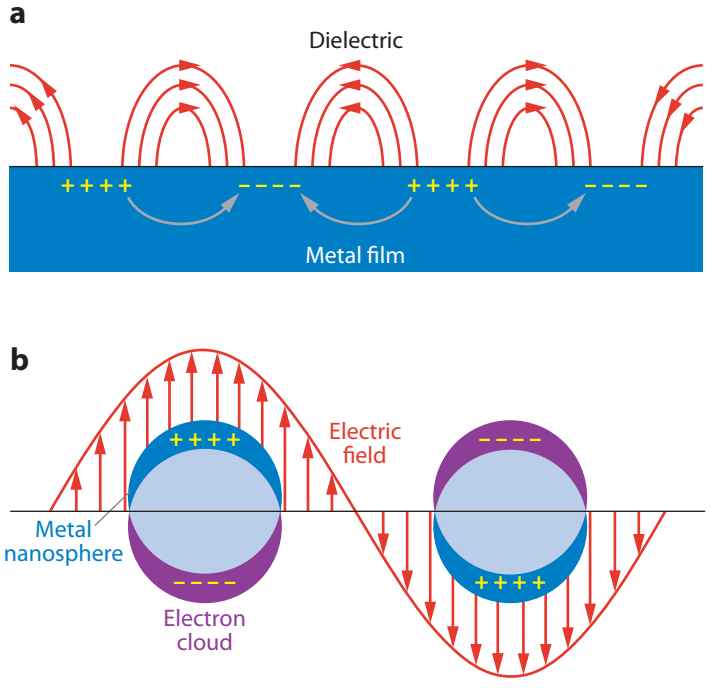

Figure 1

Depiction of (*a*) propagating surface plasmons of a metal surface and (*b*) localized surface plasmons (LSPs) of a metal nanosphere. Figure reproduced with permission from Reference 84. Copyright 2007 Annual Reviews.

plasmon is called a localized surface plasmon. The theoretical frequency of a localized surface plasmon is $\omega_p/\sqrt{3}$ for a metal sphere placed in vacuum. **Figure 1*b*** shows the interaction between the electric field of incident light and the free electrons of a metal sphere whose size is smaller than the wavelength of light. The electric field can cause free electrons to move away from the metal particle in one direction, creating a dipole that can switch direction with the change in electric field. When the frequency of the dipole plasmon is approximately the same as the incident light, a resonance condition is reached, leading to constructive interference and the strongest signal for the plasmon. Such a condition is referred to as surface plasmon resonance, or localized surface plasmon resonance (LSPR) for the case of a metal nanoparticle. For spherical nanoparticles of Au and Ag with diameters less than 30 nm, mainly dipole plasmon resonance is involved; however, for larger particles, quadrupole plasmon resonance from two negatively charged poles and two positively charged poles may be observed.

LSPR: localized surface plasmon resonance

Plasmonic nanoparticles: metal nanoparticles, with size close to or less than the wavelength of light, that display surface plasmon resonance

SERS: surface-enhanced Raman scattering

The great interest in plasmonic nanoparticles, especially for Ag and Au, is driven by their potential applications. Optical sensing, for example, exploits the change in LSPR peak position and intensity to detect binding events on Ag or Au surfaces. As the surfaces of Ag and Au nanoparticles can be readily conjugated with biologically relevant ligands, a number of detection strategies have been developed to probe biomolecules with high sensitivity and at a low cost (4–7). In addition to the scattering and adsorption of light, plasmonic nanoparticles can also be used to enhance local electromagnetic fields. LSPR can create intense local electric fields within a few nanometers of a particle surface. This near-field effect can improve Raman scattering cross sections of molecules adsorbed onto the surface. This kind of enhancement has led to the development of a new field of scientific exploration known as surface-enhanced Raman scattering (SERS) spectroscopy, with the SERS effect being first demonstrated by Fleischman and Van Duyne (8–10). Nanoscale waveguiding is another intriguing application for plasmonic nanoparticles. For example, a linear chain of Au or Ag nanoparticles with interparticle gaps less than 1 nm can channel the flow of electromagnetic energy over hundreds of nanometers, without significant loss, through the near-field coupling of the LSPR between adjacent nanoparticles. It is anticipated that centimeter-long propagation will be realized using plasmonic nanoparticles and that such structures will serve as interconnects in nanophotonic devices (11).

The first reported synthesis of plasmonic metal nanoparticles occurred more than 150 years ago when Faraday (12) prepared Au colloids by reducing an aqueous solution of Au chloride with phosphorus. Knowing that the shape of a nanoparticle can significantly affect the way it interacts with light and thus its LSPR, researchers have taken great effort to develop synthetic methods for plasmonic nanoparticles with different morphologies. During the past decade, a variety of chemical methods have been established for preparing high-quality Au and Ag nanoparticles, enabling a systematic study of LSPR dependencies on the size, shape, and structure (solid versus hollow) of metal nanoparticles. In this review, we present recent developments in the chemical synthesis of plasmonic Ag and Pd nanoparticles, emphasizing shape control. To illustrate the potential effect of shape on LSPR, we give numerical calculations for Ag nanoparticles with different shapes in the first part of this article. Following this work, we discuss how solution-phase methods can be manipulated to engineer the shape, and thus tailor the LSPR, of plasmonic nanoparticles. We focus on Ag nanoparticles (including nanocubes, right bipyramids, nanobars, nanorice, and triangular plates) because Ag has the strongest plasmonic interaction with light among all metals. As a matter of fact, the scattering cross section of Ag is a magnitude greater than that of Au (13). The syntheses of Pd nanocubes and triangular plates with LSPR in the visible region are also briefly discussed, as Pd nanoparticles compose another class of promising plasmonic nanoparticles, which have not been widely studied. We conclude by highlighting some unique properties enabled by the shape-controlled synthesis of metal nanoparticles, as well as

advantages these structures may bring to applications such as molecular detection and laser-induced heating.

Mie theory: an analytical solution to Maxwell's equations for the scattering of light radiation by small particles

DDA: discrete dipole approximation

DDA calculation: a method for computing light scattering and absorption of particles through approximation with a finite array of polarizable points

SHAPE DEPENDENCE OF LOCALIZED SURFACE PLASMON RESONANCE

The frequency and intensity of a plasmon resonance are determined primarily by (*a*) the intrinsic dielectric property of a given metal, (*b*) the dielectric constant of the medium in contact with the metal, and (*c*) the pattern of surface polarization. As such, any variation in the shape or size of a metal particle that can alter the surface polarization causes a change to the plasmon resonance. This dependence offers the ability to tailor the LSPR of metal nanoparticles through shape-controlled synthesis. The interactions of an electromagnetic wave with a nanoparticle can be understood by solving Maxwell's equations. Although exact solutions to Maxwell's equations based on analytical formulations such as Mie theory are desirable (14), such solutions are only possible for special cases such as a solid sphere, concentric spherical shells, a spheroid, and an infinite cylinder. For other particles with arbitrary geometrical shapes, numerical calculations with some approximations are required. Among available electromagnetic numerical approaches, the discrete dipole approximation (DDA) method has been widely utilized to simulate the interaction of light with metal particles of arbitrary shape (15, 16).

In the DDA method, a particle is divided into a cubic array of N polarizable points (located at $\vec{r}_i$, $i = 1, \ldots, N$), with each point representing the polarizability of a discrete volume of material. The presence of an electromagnetic field (light) gives each point a dipole moment $\vec{P}_i$ that is connected to the local electric field $\vec{E}_i$ through a quantity called polarizability α_i, namely, $\vec{P}_i = \alpha_i E_i$. The local field $\vec{E}_i$ at which the dipole $\vec{P}_i$ is excited comprises two parts: the incident field $\vec{E}_{0i}$ and the secondary radiation field $\vec{E}_i$ (which arises from all other dipole moments). Consequently, the polarization at each point ($\vec{P}_i$) must be calculated through an iterative procedure. These algorithms can be combined with the fast Fourier transform technique to greatly accelerate the numerical calculation. Once all the dipole moments $\vec{P}_i$ are solved self-consistently, they can be used to calculate the LSPR, including the scattering, absorption, and extinction cross sections (C_{sca}, C_{abs}, and C_{ext}, respectively) of a given nanoparticle as a function of wavelength. As a powerful numerical tool for investigating the effect of shape on LSPR, DDA calculations can also be integrated with experimental studies to achieve a better understanding of LSPR spectra obtained from nanoparticle samples. They can even provide some useful guidelines for the design and fabrication of new plasmonic nanoparticles.

Figure 2 compares the calculated LSPR spectra for Ag nanoparticles of various shapes suspended in water (17). The extinction, absorption, and scattering spectra for the 40-nm Ag sphere (**Figure 2*a***) were obtained using Mie theory, whereas the DDA method was used for all the other shapes. The calculated spectra for the 40-nm Ag sphere shows two resonance peaks: a main dipole resonance peak at 410 nm and a weaker quadrupole resonance at 370 nm as a shoulder. The dipole resonance arises from one side of the sphere surface being positively charged, whereas the opposite side is negatively charged, giving the particle itself a dipole moment that reverses sign at the same frequency as the incident light (18). The weak quadrupole resonance arises from energy losses that cause nonuniformity of the incident light across the sphere and the formation of two parallel dipoles of opposite sign.

The DDA-calculated extinction, absorption, and scattering spectra of a 40-nm Ag cube are shown in **Figure 2*b***. Unlike the nanosphere, the nanocube has several distinct symmetries for dipole resonance, which give rise to more peaks (19). Additionally, the position of the most intense peak for the nanocube is red-shifted compared with that of the sphere. This shift is caused by the

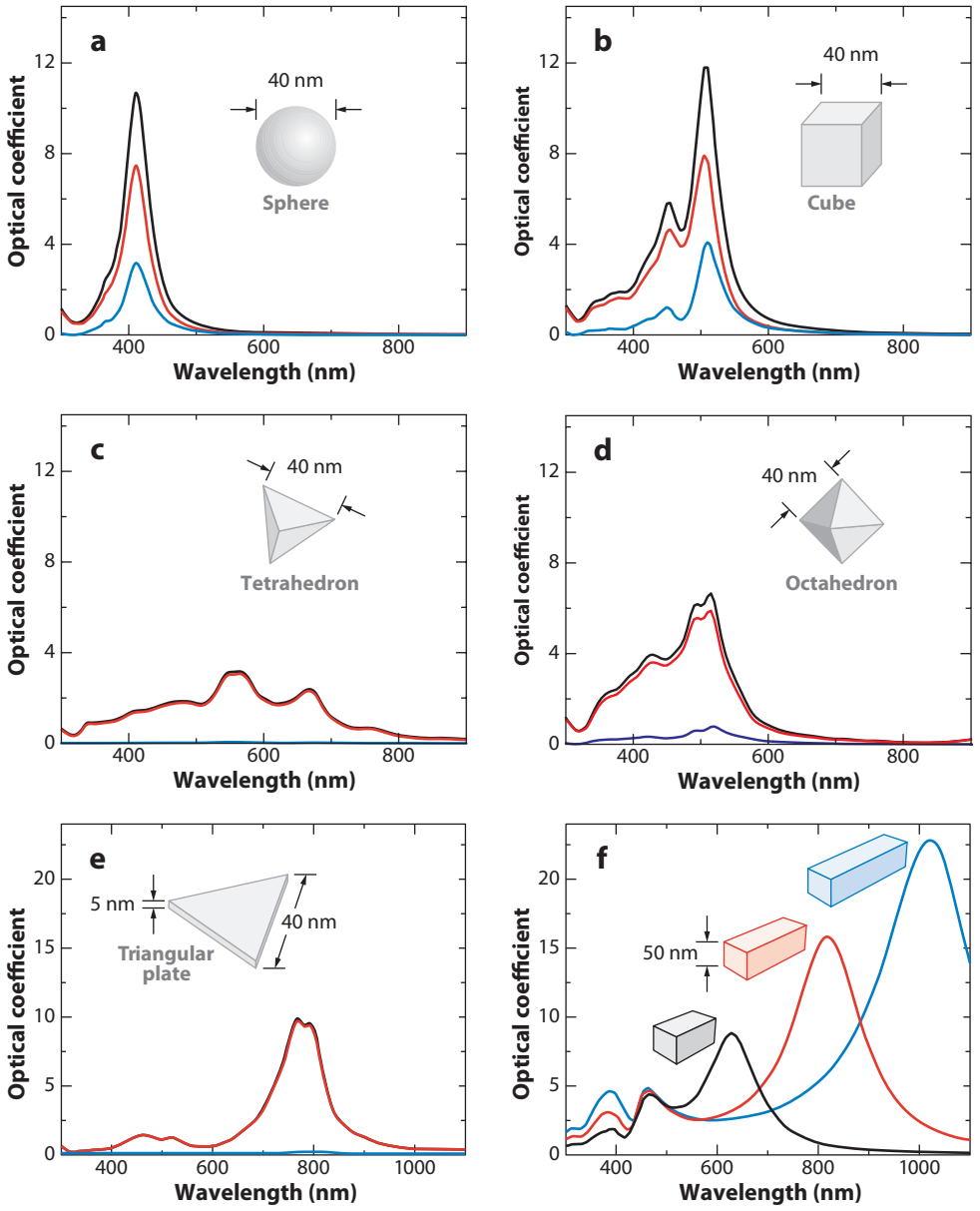

Figure 2

Extinction (*black*), absorption (*red*), and scattering (*blue*) spectra calculated for Ag nanoparticles of different shapes: (*a*) a sphere displaying a single dipole resonance peak and (*b*) a cube, (*c*) a tetrahedron, (*d*) an octahedron, and (*e*) a triangular plate. (*f*) Extinction spectra of rectangular bars with aspect ratios of 2 (*black*), 3 (*red*), and 4 (*blue*). Note that the nonspherical particles typically exhibit multiple, red-shifted resonance peaks. Panels *a–e* modified with permission from Reference 17. Copyright 2006 American Chemical Society. Panel *f* modified with permission from Reference 24. Copyright 2007 American Chemical Society.

accumulation of surface charges at the corners of the nanocube and is observed, in general, for any nanoparticle with sharp corners (20, 21). In these systems, the increased charge separation reduces the restoring force for electron oscillation, which in turn results in a shift of the resonance peak to lower energy (22). Following this trend, both a tetrahedron and an octahedron should show further red-shifted LSPR peaks because they have even sharper corners than cubes, and their simulated spectra are shown in **Figures 2*c*,*d***, respectively. **Figure 2*e*** shows the calculated spectra for a triangular plate. As a two-dimensional (2D) anisotropic structure, a triangular plate facilitates increased charge separation when polarized along one of its edges. As a result, the spectra exhibit peaks shifted toward longer wavelengths. Although sharp corners increase charge separation and result in red-shifted LSPR, the symmetry of the particle determines the intensity of dipole resonances (23). Thus, a corner-truncated triangular plate or a circular plate displays more intense peaks than a triangular plate owing to their increased symmetry; however, their primary resonances are blue-shifted relative to that of a triangular plate with sharp corners (22). The extinction spectra of 1D nanobars with different aspect ratios are shown in **Figure 2*f*** (24, 25). By controlling the aspect ratio of the nanobar, the resonance peak positions of such 1D nanoparticles can be tuned from the visible into the near infrared; this property makes nanobars and other 1D nanoparticles potentially quite versatile. Specifically, for Ag nanobars with aspect ratios of 2, 3, and 4, longitudinal polarization yields dipole resonance peaks at 700, 900, and 1100 nm, respectively, with the light-scattering intensity proportional to the aspect ratio.

Based on the DDA predictions of the LSPR spectra of different nanoparticle shapes, a number of design rules have been obtained. First, dipole resonance peaks red-shift with increasing corner sharpness and particle anisotropy. Second, the LSPR peak intensity increases with particle symmetry. Third, the number of LSPR peaks is determined by the number of ways the nanostructure can be polarized. Although it is possible to simulate spectra for complex particle shapes, only recently could metal nanoparticles of these shapes be synthetically targeted. In preparing such particles, these guiding principles for LSPR have been validated for a number of shapes.

PVP: poly(vinyl pyrrolidone)

Polyol synthesis: a versatile synthetic process for the preparation of metal nanostructures typically using a polyol as the solvent and source of reducing agent

SHAPE-CONTROLLED CHEMICAL SYNTHESIS

The past decade has witnessed the development of many methods for preparing noble-metal nanoparticles with different and well-defined shapes. All noble metals crystallize in the face-centered cubic lattice. The Wulff theorem, which has also been verified experimentally, predicts that a single-crystal, noble-metal nanoparticle assumes a truncated octahedron (or Wulff polyhedron) as its equilibrium shape in an inert gas (26–28; 29, pp. 9–11). In a solution-phase synthesis, however, the product often adopts a shape drastically different from a Wulff polyhedron because of the anisotropic interactions of different facets with capping agents and solvent, the formation of twin structures with energies lower than that of a cuboctahedron, and/or the use of an elevated reaction temperature. These attributes make solution-phase methods more powerful and versatile than vapor-phase methods for the shape-controlled synthesis of noble-metal nanoparticles. Among the various solution-phase methods, polyol reduction is probably the best established for generating Ag and Au nanoparticles with controllable shapes and optical properties (30–35). In a typical synthesis, ethylene glycol serves as both the solvent and source of reductant, generating metal atoms from a salt precursor at an elevated temperature (36–38). The formation of nanoparticles with controlled shapes is facilitated by adding a polymeric capping agent, typically poly(vinyl pyrrolidone) (PVP), to a polyol synthesis. It has been established that the shape taken by a noble-metal nanoparticle is determined primarily by the number of twin defects included in the initial seed. Different seeds can then grow into nanoparticles having different shapes (**Figure 3**) (39). For example, a single-crystal seed can grow into an octahedron or cube (with

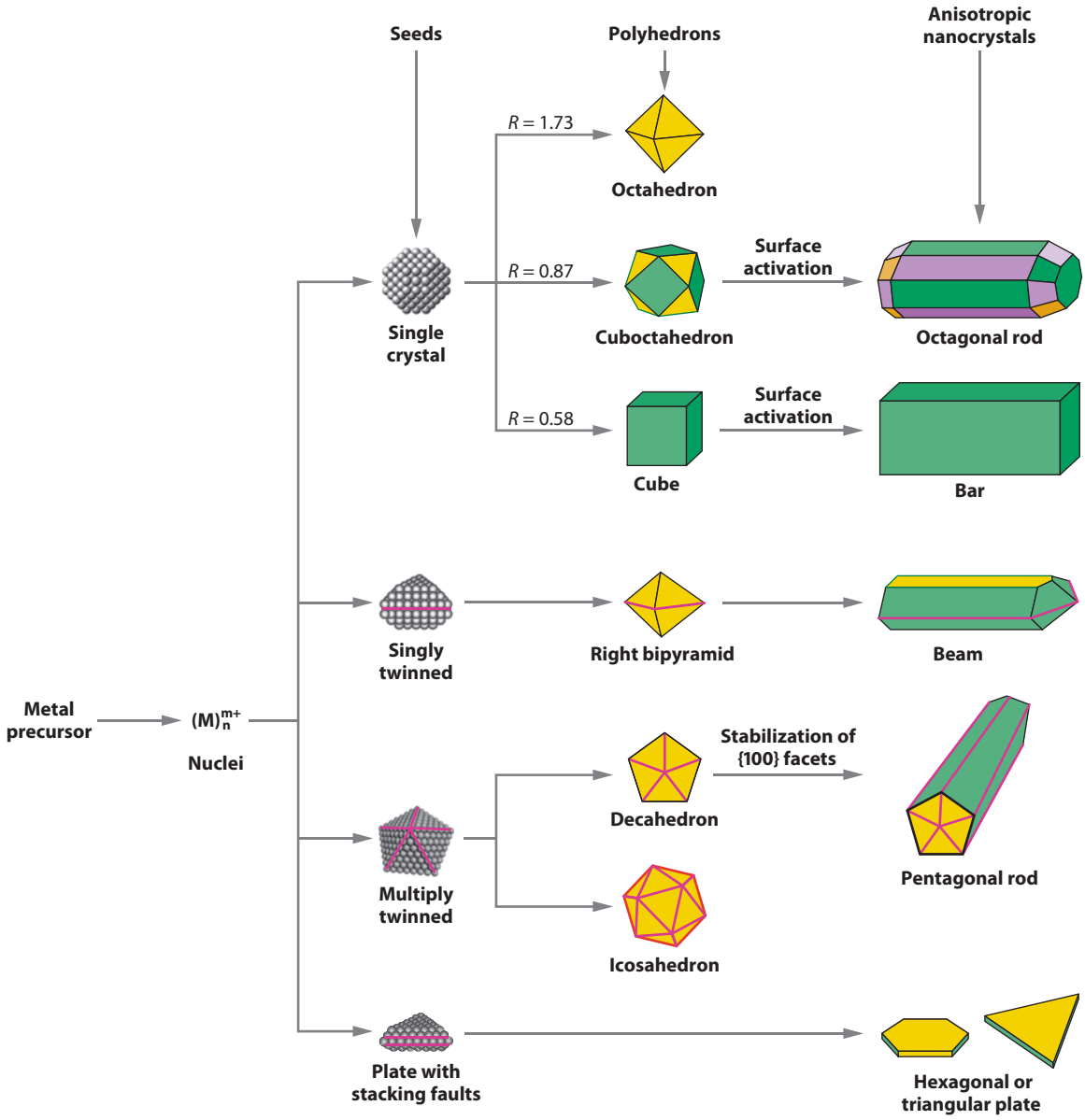

Figure 3

A schematic illustrating the reaction pathways that lead to noble-metal nanoparticles having different shapes. First, a precursor is reduced or decomposed to form nuclei (small clusters). Once the nuclei have grown past a certain size, they become seeds with a single-crystal, singly twinned, or multiply twinned structure. If stacking faults are introduced, plate-like seeds form. Green, orange, and purple represent the {100}, {111}, and {110} facets, respectively. The parameter *R* is defined as the ratio between the growth rates along the ⟨100⟩ and ⟨111⟩ directions. Twin planes are delineated in the drawing with magenta lines. Figure modified with permission from Reference 39. Copyright 2007 Wiley-VCH.

varying degrees of corner truncation) by controlling the relative growth rates along the ⟨100⟩ and ⟨111⟩ directions; such control is typically achieved through the introduction of a capping agent (40). Additionally, single-crystal cuboctahedrons and cubes can be made to grow anisotropically into 1D nanorods with octagonal cross sections and nanobars with rectangular cross sections, respectively, by the activation of a specific side face through oxidative etching. From singly twinned seeds, right bipyramids or nanobeams are typically produced, whereas multiply twinned seeds with a decahedral shape can be directed to grow into rods or nanowires with a pentagonal cross section. Finally, plate-like seeds grow into hexagonal and then eventually triangular plates.

Oxidative etching: a method to control the crystalline structure of seeds through the introduction of an oxidative etchant during the chemical synthesis of nanoparticles

From these examples, it becomes apparent that to prepare plasmonic nanoparticles of one desired shape, it is critical to control the internal structures of the seeds. In a solution-phase synthesis, small clusters of metal atoms can fluctuate between single-crystal and twinned morphologies at typical reaction temperatures (41). Because of this fluctuation, the synthesis usually generates a mixture of single-crystal and twinned noble-metal structures. Thus, to form single-crystal structures exclusively, twinned seeds must be selectively removed. Investigators have controlled the distribution of seed structures produced in solution in a number of ways, such as oxidative etching and kinetic control (25, 39). Here, we consider the synthesis of Ag and Pd nanostructures as model systems with regard to how these methods can be applied to prepare plasmonic nanoparticles with various shapes and LSPR features.

The Case of Silver

Oxidative etching can remove multiply twinned seeds from solution and therefore promote the formation of single-crystal nanoparticles. With this approach, an etchant, such as Cl^-, is introduced into the synthesis to selectively etch away seeds containing twin defects. The selective etching of twin defects is enabled because the defect sites are more reactive than single crystalline regions (42). This method has been successfully applied to the preparation of Ag nanocubes using a polyol method in which $AgNO_3$ is reduced in ethylene glycol, with PVP serving as a polymeric capping agent (33, 43, 44). The reaction is performed in air, with Cl^- introduced through the addition of NaCl or HCl. Close monitoring of the reaction process by UV-visible spectroscopy and electron microscopy revealed that twinned particles are formed first but later dissolved by oxidative etching. Thus, after a certain reaction time, single-crystal seeds with a spherical profile predominate (**Figure 4*a***). If the reaction is then allowed to continue, the cuboctahedral seeds grow into nanocubes with all facets being {100} (**Figure 4*b***). Both Cl^- and O_2 are required to form single-crystal seeds, indicating the oxidative etching reaction mechanism, whereas PVP helps to stabilize the {100} facets of the nanocubes. Oxidative etching has also been validated for other noble metals, including Pd, Pt, and Rh (45–48).

The extinction spectra of sharp nanocubes suspended in water exhibit several distinct dipole resonances (**Figure 4*c***). For 90-nm nanocubes, the most intense resonance peak is at 600 nm, which is red-shifted compared with Ag spheres and truncated nanocubes of similar size, which have peaks positioned at 440 and 500 nm, respectively (33, 43). The other observed dipole resonances for sharp nanocubes can be attributed to particle anisotropy and are consistent with the DDA calculations. In general, the number of peaks observed correlates with the number of ways in which the nanoparticle can be polarized.

The oxidative etching process used to synthesize the nanocubes can also be manipulated to prepare other novel nanoparticles. For example, if a less corrosive etchant (such as Br^- instead of Cl^-) is added to the reaction, only the most reactive multiply twinned seeds are removed from the reaction, leaving behind both singly twinned and single-crystal seeds (49). **Figure 4*d*** shows a high-resolution transition electron micrograph of a singly twinned seed found in the reaction

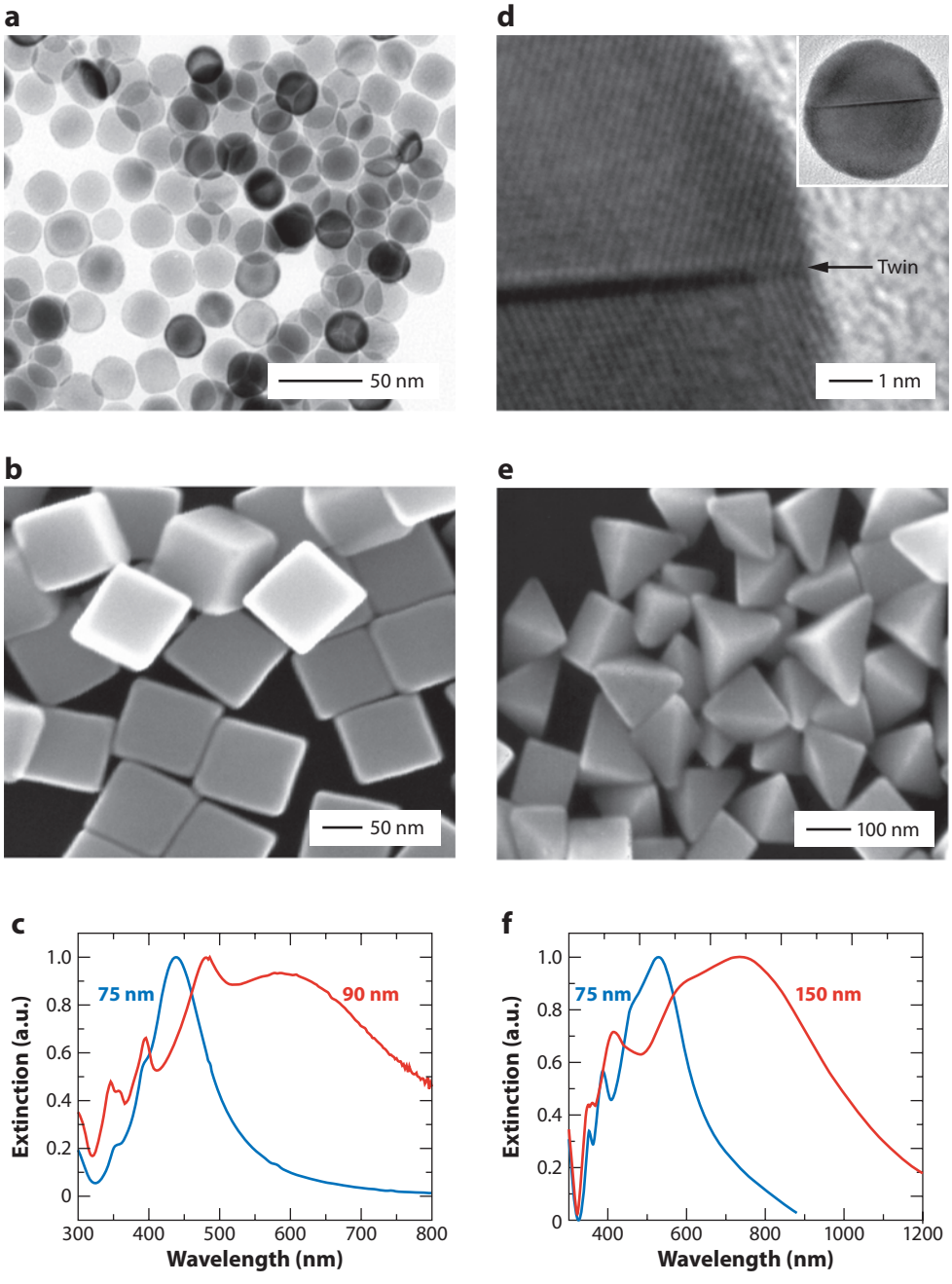

Figure 4

(*a*) Transmission electron micrograph and (*b*) scanning electron micrograph of single-crystal seeds responsible for the formation of Ag nanocubes. (*d*) High-resolution image and (*e*) scanning electron micrograph of a singly twinned seed involved in the formation of Ag right bipyramids. (The inset of panel *d* shows a typical transmission electron micrograph.) Localized surface plasmon resonance spectra taken from aqueous suspensions of (*c*) Ag nanocubes and (*f*) Ag bipyramids (two different sizes for each shape). Figure modified with permission from Reference 17. Copyright 2006 American Chemical Society.

sample at 1.5 h. These singly twinned seeds can then grow into right bipyramids, with their edge lengths increasing with reaction time. **Figure 4*e*** shows a scanning electron micrograph for 150-nm right bipyramids obtained at a reaction time of 5 h. Similar to Ag nanocubes, the Ag bipyramids are bound by {100} facets, but in contrast, they contain a (111) twin plane that bisects their two tetrahedral halves. The unique shape of the right bipyramid gives it a distinct LSPR spectrum. **Figure 4*f*** shows normalized extinction spectra for right bipyramids with edge lengths of 75 and 150 nm. Notably, the most intense peak shifted from 530 to 742 nm with the increase in edge length, which can be attributed to the increase in charge separation and energy loss for the larger particle. Additionally, compared with nanocubes, the corners of the bipyramids are significantly sharper, leading to a red shift of the main resonance peak relative to nanocubes of similar size. Such sharp corners also cause higher localized field enhancement, making right bipyramids promising substrates for SERS.

The concentration of corrosive anions also plays a critical role in controlling the shape of Ag nanoparticles produced during a polyol synthesis. For example, if the molar ratio of Br^- to Ag is increased from 1:850 to 1:425, single-crystal nanobars with rectangular side facets (**Figure 5*a***) are formed instead of nanocubes; the nanobars have an average aspect ratio of 2.7 (24). In the previous example, Br^- could effectively etch away multiply twinned seeds produced at early stages of a reaction; in this case, increasing the concentration of Br^- enhances oxidative etching, promoting the formation of single-crystal instead of singly twinned seeds; however, the exact mechanism behind the anisotropic growth is unclear, particularly given that all the side facets are identical. Interestingly, Br^- also facilitates the formation of Pd nanobars, Pd nanorods, and Au nanorods, indicating that it is likely the key ingredient for inducing such anisotropic growth (50, 51).

Unsurprisingly, the Ag nanobars exhibit some fascinating optical properties as predicted by the DDA method. The visible-near-infrared scattering spectra of individual nanobars with different aspect ratios show two resonance peaks, with one transverse plasmon resonance peak in the blue region at ~460 nm and one longitudinal plasmon resonance peak in the visible or near-infrared region (**Figure 5*b***). The location of the longitudinal plasmon resonance peak is highly dependent on the aspect ratio of an individual nanobar, which is consistent with the DDA calculations shown in **Figure 2*f***. Still, the position of the longitudinal resonance for an individual nanobar with a particular aspect ratio is always slightly blue-shifted relative to that predicted by the DDA calculations; we attribute this discrepancy to the slightly rounded corners and edges of nanobars prepared synthetically. Indeed, transforming the nanobars into nanorice by aging them in an aqueous solution of PVP for 1 week gives single-crystal nanorice (**Figure 5*c***) with substantially blue-shifted plasmon resonances for both transverse and longitudinal modes (**Figure 5*d***). Such blue shifts have also been observed when other nanoparticle shapes are aged, and this observation is consistent with DDA calculations (17, 52, 53). The light-scattering efficiency of Ag nanoparticles smaller than 60 nm is believed to be twice that of Au (54, 55). Considering the limited success with regard to the synthesis of Ag nanorods (56), especially in contrast to Au nanorods (57–61), nanobars and nanorice represent an important class of Ag nanoparticles that could potentially compete with Au nanorods for optical imaging.

Triangular plates represent another important class of Ag nanoparticles. The sharp corners and edges of triangular Ag plates generate a maximum electromagnetic-field enhancement, making these nanoparticles attractive for various spectroscopic techniques (16, 23). Despite substantial efforts dedicated to the preparation of Ag nanoplates, the ability to grow triangular Ag plates with controllable sizes and in high yields remains a challenge (62–70). This difficulty exists because the formation of plate-like seeds in solution is not thermodynamically favored owing to their large surface areas and extremely high total free energy as compared with polyhedral seeds. To form plate-like seeds in solution, one must achieve kinetic control to slow down the formation

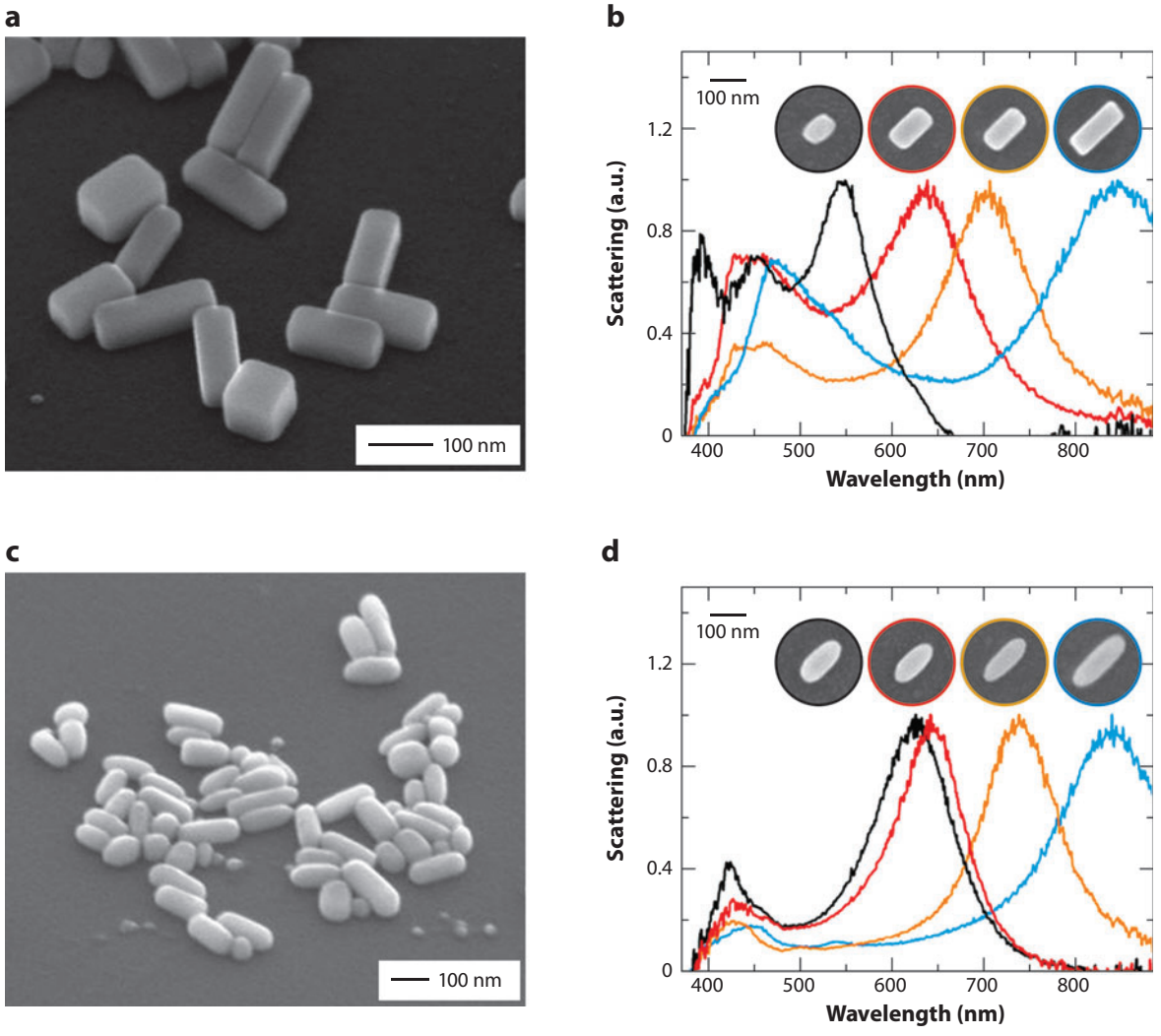

Figure 5

Scanning electron micrographs of (*a*) Ag nanobars (45° tilt) synthesized using polyol reduction in the presence of 0.11-mM NaBr, (*b*) individual Ag nanobars with their corresponding dark-field scattering spectra, (*c*) Ag nanorice (45° tilt) derived from the nanobars via an aging process, and (*d*) individual Ag nanorice with their corresponding dark-field scattering spectra. Figure modified with permission from Reference 24. Copyright 2007 American Chemical Society.

of metal atoms and/or clusters. In doing so, the plate-like seeds form through random hexagonal close-packing, thus avoiding the thermodynamically favored polyhedral seeds. To achieve kinetic control, a weak reducing agent such as PVP can be used to prepare Ag plates from $AgNO_3$ in aqueous solution (71). PVP has been used as the capping agent in the polyol syntheses of nanocubes, right bipyramids, and nanobars (33, 72). In the case of nanoplates, the hydroxyl (-OH) end groups present in commercially available PVP are critical for reduction to occur (73). **Figure 6*a–c*** shows scanning electron micrographs of Ag plates obtained at different reaction times, with an evolution from circular plates into triangular ones observed with increased reaction time. Once formed, the triangular plates can grow to 250 nm in edge length.

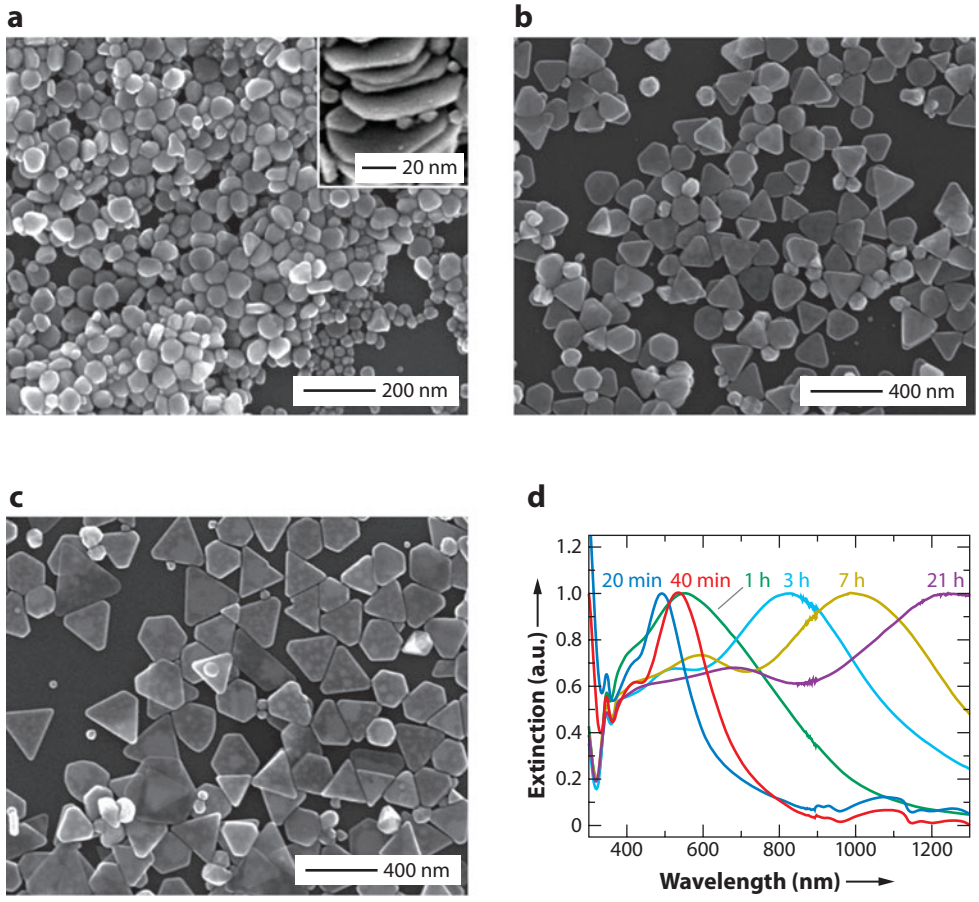

Figure 6

Kinetically controlled synthesis of Ag triangular nanoplates through reduction by the hydroxyl end groups of poly(vinyl pyrrolidone). Scanning electron micrographs of products sampled at different stages of a synthesis: (*a*) $t = 40$ min, (*b*) $t = 3$ h, and (*c*) $t = 7$ h. (*d*) UV-visible spectra of these products dispersed in water. The inset of panel *a* shows a scanning electron micrograph of some stacked plates. Figure modified with permission from Reference 71. Copyright 2006 Wiley-VCH.

Figure 6*d* plots the plasmon resonance spectra of Ag plates obtained at different reaction times using the PVP reduction method. The position of the extinction peaks gradually red-shifted into the near-infrared region with increased reaction time, which correlates with the increase in edge length. The most intense peak of each spectrum can be attributed to the in-plane dipole resonance of the nanoplates, whereas the shoulders correspond to their out-of-plane resonance. A detailed mechanic study of Ag nanoplate formation showed that the amount of $AgNO_3$ that can be reduced is directly proportional to the number of PVP chains, indicating that the hydroxyl end groups play a key role in the formation of triangular plates. Also, it was discovered recently that aqueous solutions made of commercially available $AgNO_3$ contain an abundant amount of trimeric clusters (74). These clusters, either positively charged (Ag_3^+) or neutral (Ag_3), have a stronger affinity for electrons than Ag^+, making them more favorable sites for nucleation and growth during the reduction. As a result, the final size of Ag nanoplates prepared by reduction

with PVP is also dependent on the concentration of the trimeric clusters present in the early stages of reaction.

The Case of Palladium

Unlike Ag and Au, the shape effect of Pd nanoparticles on LSPR remains largely unexplored. Based on DDA calculations, the resonance peak of Pd can be tuned from the UV (330 nm) to the visible region (530 nm) by tuning the shape of a Pd nanoparticle from a cube to an icosahedron and then a triangular plate (16, 23, 75). The synthesis of Pd nanoparticles with well-controlled shapes has been challenging, but as with the Ag system, maneuvering the crystallinity of Pd seeds holds the key. Control over the distribution of single-crystal and multiply twinned Pd seeds produced in solution can be achieved through kinetic control and/or oxidative etching. It has been shown experimentally that slow reduction favors the formation of Pd seeds with twin defects, whereas high reduction rates promote the formation of single-crystal seeds (39). Additionally, oxidative etching can increase the proportion of single-crystal seeds at early stages of a reaction, thus increasing the yield of single-crystal nanoparticles in the final product.

Based on this strategy, various single-crystal Pd nanoparticles (including Pd cuboctahedrons, nanocubes, nanobars, and nanorods) and twinned Pd nanoparticles (such as Pd icosahedrons, fivefold twinned rods, singly twinned right bipyramids, and triangular plates) have been prepared in high yields by solution-phase methods (39, 45, 46, 50, 73, 76–78). **Figure 7** shows transmission electron micrographs of Pd nanocubes and nanoplates with LSPR peaks tuned to the visible region. The Pd nanocubes are stabilized with PVP (46) and were prepared through the reduction of Na_2PdCl_4 at 90°C in ethylene glycol; $FeCl_3$ was added to the synthesis as an oxidative etchant. By varying the concentration of $FeCl_3$, the size of the cubes could be tuned from 8 to 50 nm. Although the LSPR peaks of Pd cubes with edge lengths less than 25 nm are located in the UV region, increasing the size of the Pd cubes to 50 nm results in a red shift into the visible, with a resonance peak at 390 nm (**Figure 7*b***). When HCl was added to the synthesis and the temperature was reduced slightly to 85°C, the etching power of the Cl^-/O_2 pair was enhanced, thus reducing the reduction rate of Na_2PdCl_4. As a result, the product was predominated by either triangular or hexagonal plates, depending on the concentration of $FeCl_3$ used (76). Compared with the LSPR spectra of Pd nanocubes, the Pd nanoplates display LSPR peaks shifted toward longer wavelengths, which is consistent with the greater charge separation achieved by the nanoplate morphology. For example, the extinction spectrum for triangular plates with an edge length of 25 nm and a thickness of 5 nm is in the visible region, centered at 520 nm (**Figure 7*d***). The extinction spectrum for hexagonal Pd plates of similar size also has an LSPR peak red-shifted as compared with the Pd nanocubes (**Figure 7*d***). Pd nanoparticles with LSPR peaks in the visible region may serve as ideal SERS substrates. An initial study of the SERS activity of Pd plates showed great promise for the detection of molecular species, most likely enabled by their red-shifted LSPR and sharp corners and edges (79–81). Because Pd is highly sensitive to hydrogen, the plasmonic Pd nanoparticles may be especially useful for LSPR-based detection of hydrogen gas (82, 83).

APPLICATIONS

The shape-controlled synthesis of metal nanoparticles is far beyond a scientific curiosity. The development of a library of plasmonic nanoparticles with distinct shapes and thus LSPR spectra could be particularly useful for a wide range of applications, including biological labeling, photothermal therapy, LSPR sensing, and SERS (1, 20, 84–86).

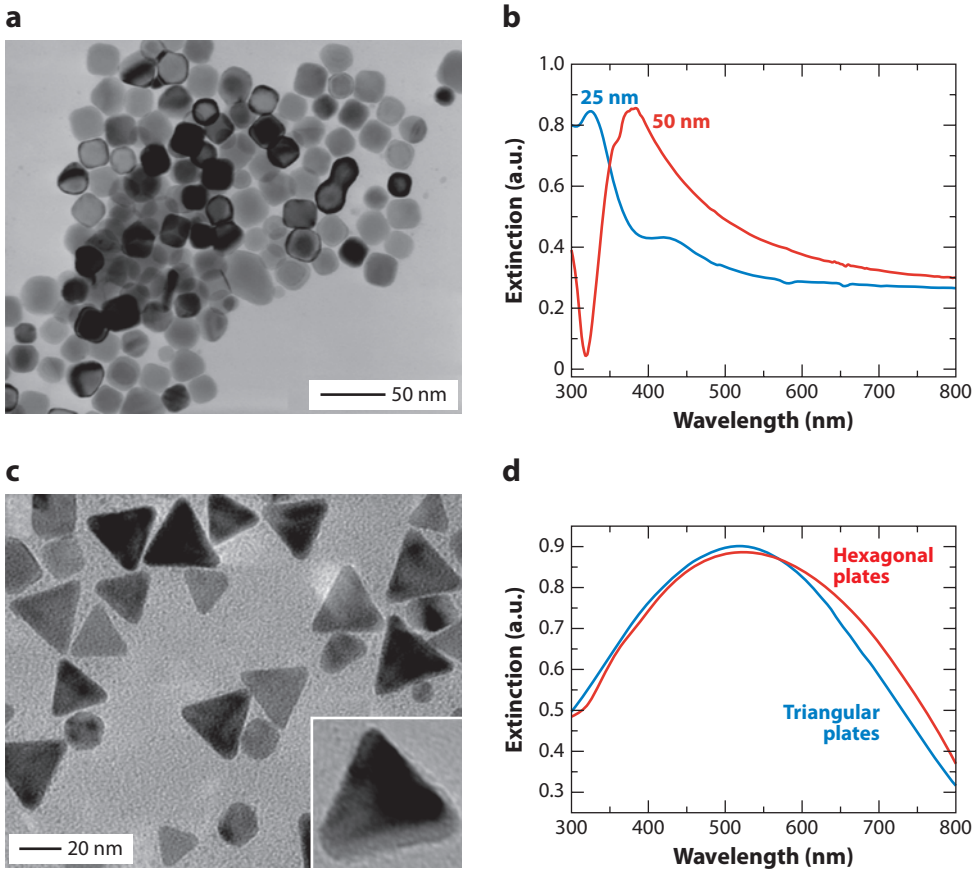

Figure 7

(*a*) Transmission electron micrograph of 25-nm Pd nanocubes prepared in the presence of 0.5-mM $FeCl_3$. (*b*) UV-visible spectra of Pd nanocubes with an average edge length of 25 and 50 nm. (*c*) Transmission electron micrograph of triangular Pd nanoplates prepared at 85°C in the presence of 0.36-mM $FeCl_3$ and 5-mM HCl, with a molar ratio of poly(vinyl pyrrolidone) (in terms of repeating unit) to Pd precursor of 5. (*d*) UV-visible spectra of the as-prepared triangular and hexagonal Pd nanoplates. Panels *a* and *b* modified with permission from Reference 46. Copyright 2005 American Chemical Society. Panels *c* and *d* modified with permission from Reference 76. Copyright 2005 American Chemical Society.

Surface-Enhanced Raman Scattering Measurement of Silver Nanocubes Suspended in Solution

Although the phenomenon of SERS was first observed in the 1970s, only recently has SERS achieved a significant level of understanding, both theoretically and experimentally (87, 88). It is well-known that the SERS enhancement factor (EF) of a metal nanoparticle is strongly dependent on the shape of the particle. This dependence can be understood in terms of (*a*) the LSPR properties (including the number, spectral position, and intensity of the resonance modes) of a metal nanoparticle being highly sensitive to its shape and symmetry (23, 89) and (*b*) the sharp corners on the surface of a nanoparticle being able to create a greater localized electric field in comparison to rounded ones (53). Thus, controlling the shape of plasmonic nanoparticles plays an important role in maximizing the EF for SERS.

EF: enhancement factor

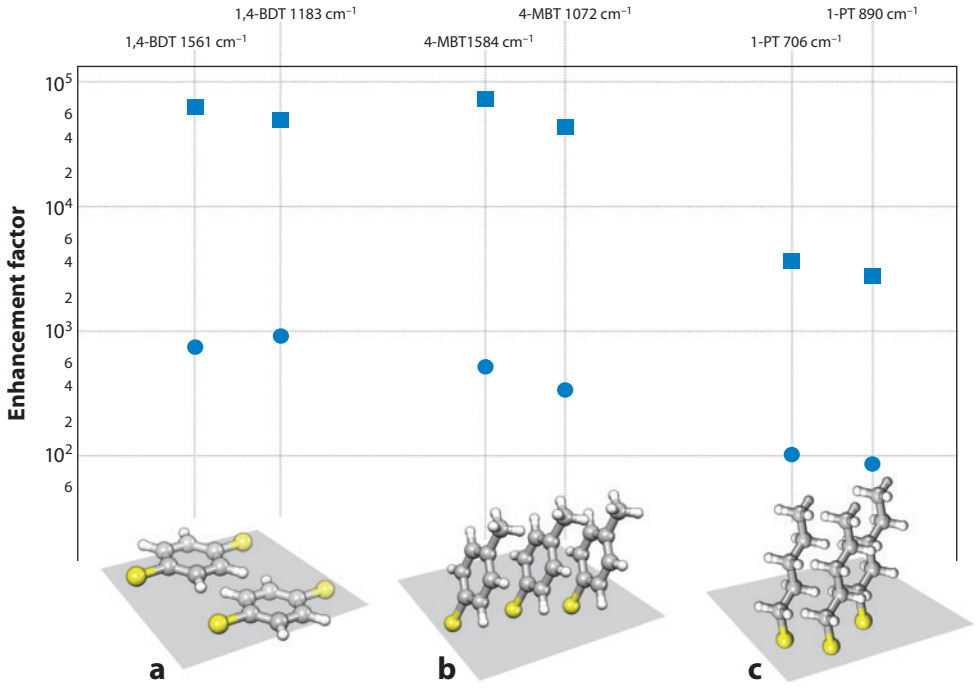

Figure 8

Enhancement factors measured for Ag nanocubes (*squares*) and nanospheres (*circles*) calculated with (*a*) the 1561 cm^{-1} and 1183 cm^{-1} bands of 1,4-benzenedithiol (1,4-BDT), (*b*) the 1584 cm^{-1} and 1072 cm^{-1} bands of 4-methyl benzenethiol (4-MBT), and (*c*) the 706 cm^{-1} and 890 cm^{-1} bands of 1-pentanethiol (1-PT). All experiments used a 514-nm laser and were performed in water. The schematic at the bottom represents the approximate orientation of the molecules on the metal surface (M. Rycenga & Y. Xia, submitted manuscript).

Figure 8 shows the SERS EFs obtained when similarly sized Ag nanospheres and Ag nanocubes were used as substrates in aqueous solutions. The EF provided by each particle was calculated for three molecules: 1,4-benzenedithiol, 4-methyl benzenethiol, and 1-pentanethiol. The measurements represent an average EF, and a comparison between the nanospheres and nanocubes revealed that the sharp corners of the cubes enabled greater enhancement of Raman signals than nanospheres. This experiment fits well with theory and illustrates the importance of controlling nanoscale features for SERS applications in which the greatest enhancement is desired.

Sharp features are important for maximizing the SERS EF, but the LSPR properties of the enhancing metal features must also be considered. SERS is a near-field effect and occurs when incident light is in resonance with an LSPR mode of a metal nanoparticle or roughened thin film (90). Excitation of the LSPR mode results in selective absorption and scattering of the incident light and the generation of strong electromagnetic fields at the metal surface. SERS requires that analyte molecules be confined within these electromagnetic fields, but not necessarily adsorbed to the metal surface. Typically, the SERS EF can range from 10^4 to 10^{11} (91), with the exact magnitude strongly dependent on experimental parameters, including the LSPR or surface plasmon resonance of the metallic feature. Still, despite this understanding, there are often discrepancies in the literature with regard to the actual EF provided by a particular metal structure. To bring more uniformity to the field, metal nanoparticles with well-controlled shapes and sizes serve as an ideal system to probe more thoroughly the underlying principles of SERS.

SERS EF: improvement in Raman scattering of molecules absorbed on a metal surface; an EF of 1014 ~ 1015 is desired for single-molecule detection

Localized Surface Plasmon Resonance and Surface-Enhanced Raman Scattering Measurement of Supported Silver Nanocubes

In many applications, it is desirable to support plasmonic particles on a substrate, which can alter their LSPR properties. **Figure 9*a*** shows LSPR spectra measured from an ensemble of Ag nanocubes and a single Ag nanocube supported on a glass substrate. Both samples were in an aqueous environment. The small side peak in the ensemble spectrum results from quadrupole excitations, whereas the main ensemble peak results from dipole excitations of nanocubes completely immersed in an H_2O environment. The single-particle spectrum contains a resonance that is absent from the ensemble spectrum. This different spectral response is observed because

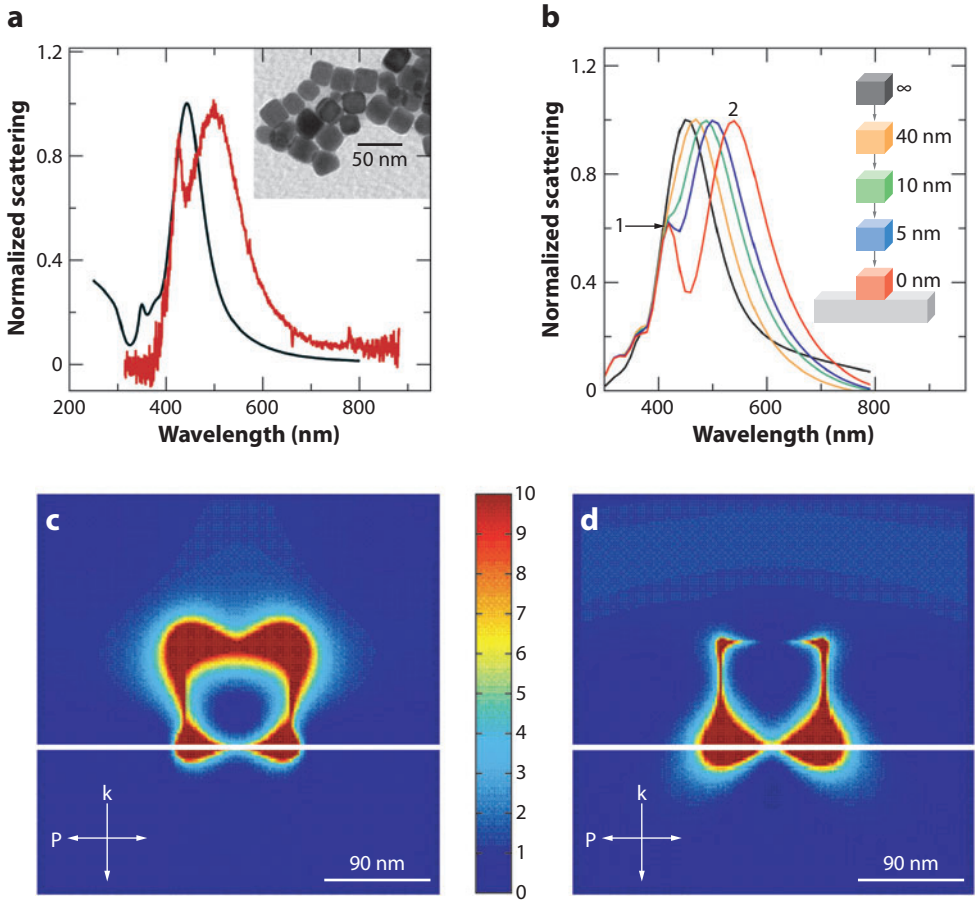

Figure 9

(*a*) Localized surface plasmon resonance spectra of nanocube ensemble extinction (*black*) and single nanocube dark-field scattering supported on a glass substrate (*red*). Finite-difference time-domain calculations showing (*b*) the emergence of a second resonance peak as an Ag nanocube (90 nm in edge length) approaches a dielectric substrate and the field intensities for (*c*) peak 1 and (*d*) peak 2 of the nanocube in contact with the substrate (the *white line* in the field pattern images represents the substrate). Figure modified with permission from Reference 92. Copyright 2005 American Chemical Society.

the supported single nanocube is in contact with a second dielectric environment, with a higher dielectric constant (a glass coverslip), in addition to its water environment. This second dielectric environment creates two dipole resonant conditions for the two dielectric environments. The higher dielectric (glass) yields the lower energy resonance, which is red-shifted from the ensemble dipole resonance, and the lower dielectric (water) yields the higher energy resonance, which falls within the range of the ensemble dipole resonance because these two resonances are a result of the same dielectric medium. This argument is verified by a number of calculations with the cube suspended at various heights over the substrate until they come into contact. **Figure 9*b*** shows the result of a finite-difference time-domain calculation that simulates the proximity effect of a nanocube approaching a dielectric substrate. As the nanocube approaches the substrate, the symmetry of the environment surrounding the cube is lost, causing its dipole resonance to broaden and split into two peaks: one at 430 nm that is associated with the large fields away from the substrate and a second peak at 550 nm that is associated with the large fields toward the substrate. **Figures 9*c*,*d*** show a side view of the field intensity for peak 1 and 2, respectively, when the cube is touching the surface. This new peak is extremely sensitive to changes in its environment, which makes it ideal for sensing applications based on changes in refractive index (92).

Supported nanocubes can also act as sensing platforms for SERS. Our recent study using Ag nanocubes on an Si substrate confirmed their SERS activity and revealed how sensitive SERS is to the geometry of nanoscale features (93). Unlike measurements in solution, when nanocubes are supported, they have a fixed orientation relative to the laser polarization. **Figure 10** shows the effects of laser polarization on the local electric field of a nanocube. The results show that when a nanocube is irradiated with light polarized in the [100] direction, the electric field collects at all corners of the cube (**Figure 10*a***); however, when the light is polarized in the [110] direction, accumulation occurs only along the diagonal (**Figure 10*b***). This polarization dependency also affects the local electric-field intensity. For the cube, the maximum electric-field amplitude $|E|_{\max}$ at [100] polarization is 26.5, whereas the value is 37.8 for [110] polarization. This result indicates that the [110] polarization could generate a peak enhancement approximately four times that of the [100] polarization as SERS is proportional to $|E|^4$. Because the field is not uniformly distributed, the field amplitude averaged over the entire surface of the particle is perhaps a more useful value for predicting the SERS EF of a single particle. In this case, the average $|E|^4$ values for the [100] and [110] polarizations are 2653 and 5154, respectively. Compared with a nanosphere (**Figure 10*c***), the nanocube has a much larger electric-field intensity owing to its sharp corners. These calculations not only demonstrate the importance of particle shape in controlling the distribution of near fields, but also suggest that the SERS signals can vary drastically if the particle is not spherical and positioned at different orientations relative to the laser polarization.

This angular dependence simulation has been verified experimentally with Ag nanocubes. To ensure that the observed signal enhancement corresponded with a particular laser polarization, Ag nanocubes were cast onto Si wafers patterned with registration marks that could be observed in both the scanning electron microscope and Raman instrument. An example of one such substrate is shown in **Figure 11**. Using a custom-designed stage, one could rotate a selected particle while collecting SERS spectra. The results are shown in **Figure 12** for an Ag nanocube at different azimuthal angles relative to laser polarization, with 1,4-benzenedithiol used as the probe molecule. Notably, when the cube was oriented with a diagonal axis parallel to laser polarization (**Figure 12*a*,*c***), the Raman signal from 1,4-benzenedithiol at 1565 cm^{-1} was much greater than when the cube was oriented with one face parallel to laser polarization (**Figure 12*b***). When the

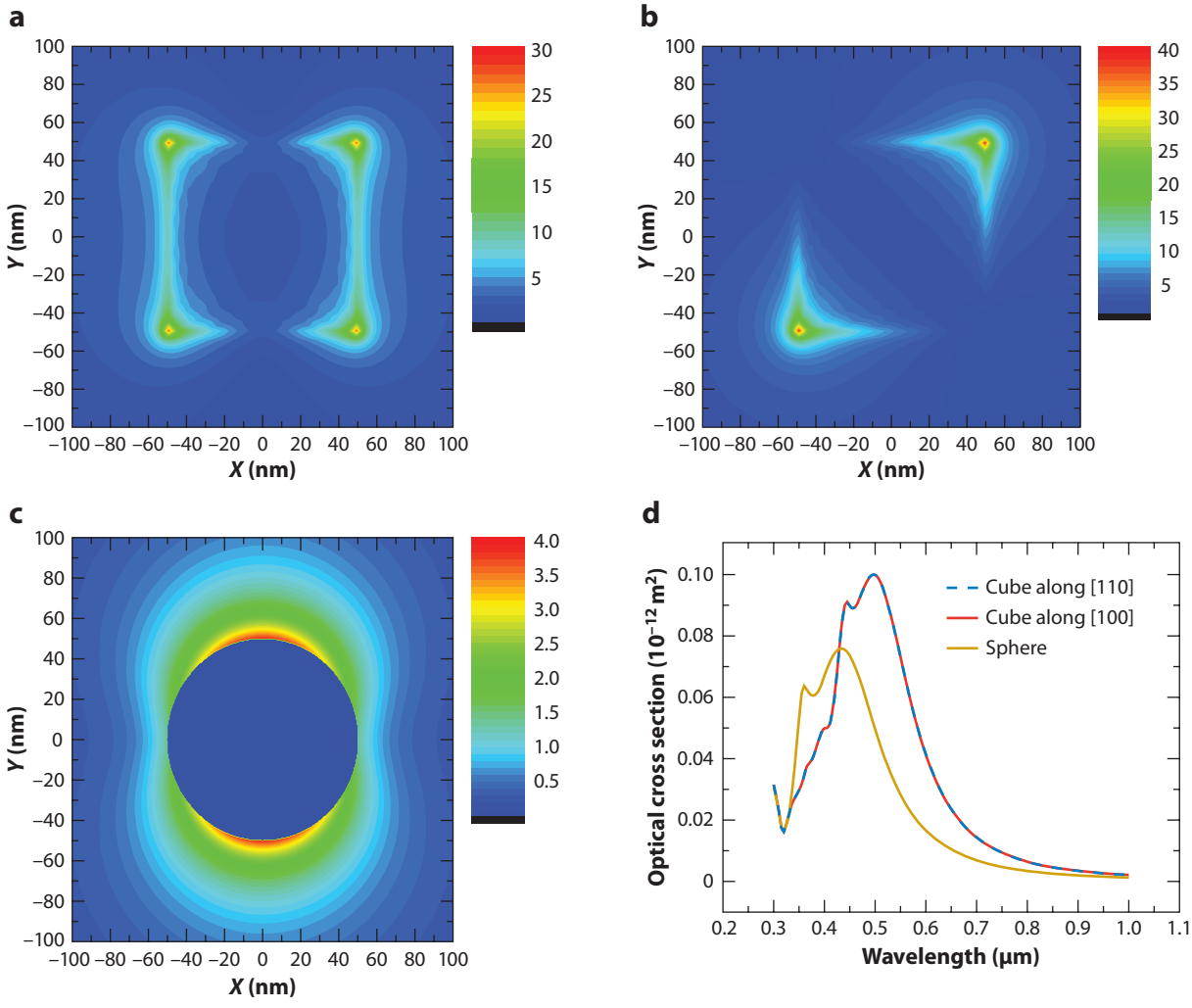

Figure 10

Electric-field amplitude (|*E*|) patterns for a 100-nm Ag cube at two polarizations and a 100-nm Ag sphere when irradiated at wavelength of 514 nm: (*a*) a 100-nm Ag cube, with the incident light along the *z* axis and the electric field along the *x* axis or [100] direction, (*b*) a 100-nm Ag cube, with the incident light along the *z* axis and electric field along the [110] direction, and (*c*) a 100-nm Ag sphere, with the incident light along the *z* axis and electric field along the *x* axis. The incident field amplitude was assumed to be 1. (*d*) Far-field extinction spectra calculated for a 100-nm Ag sphere in air (*solid orange line*) and a 100-nm Ag cube excited at two polarizations: [110] (*blue dashed line*) and [100] (*solid red line*). All spectra were calculated for particles suspended in air. Figure reproduced with permission from Reference 93. Copyright 2007 American Chemical Society.

same experiment was conducted on a highly truncated cube, the SERS spectra were unaffected by laser polarization (**Figure 12*d–f***). These results are consistent with the calculated electric-field amplitude patterns shown in **Figure 10**.

In principle, one can adjust numerous parameters to increase the SERS EF, but shape control seems to be the most effective route. Now that the relationship between the LSPR of a nanoparticle and its shape and composition is understood reasonably well, it becomes possible to predict

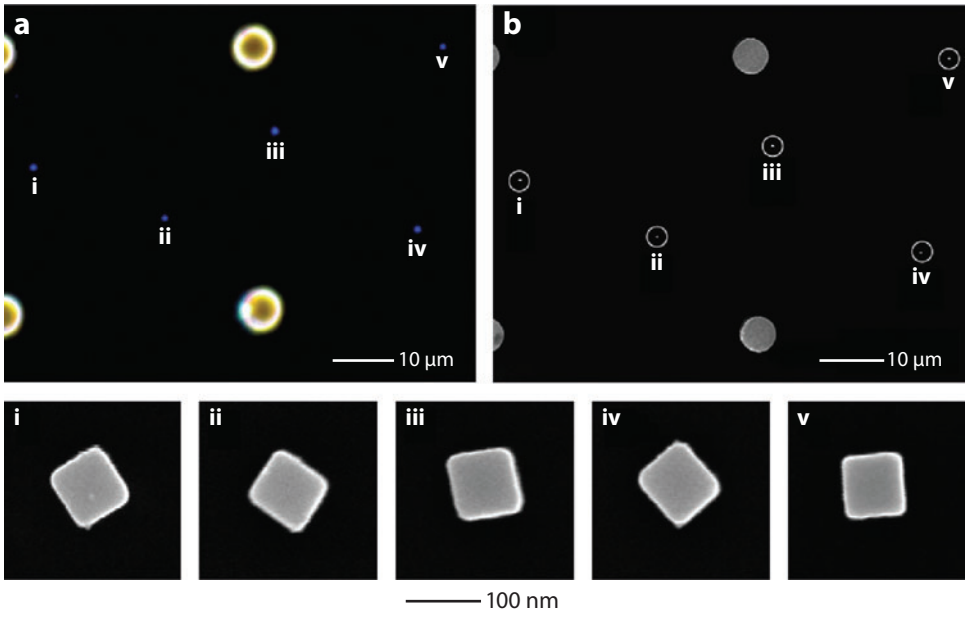

Figure 11

(*a*) Dark-field optical micrograph of a substrate with registration marks (*large yellow spots*) and a number of individual Ag nanocubes (*small blue dots*). (*b*) The corresponding scanning electron micrograph of the same region in panel *a*. (*i–v*) Scanning electron micrographs of each individual Ag nanocube. Figure reproduced with permission from Reference 93. Copyright 2007 American Chemical Society.

the near- and far-field properties of particular nanoparticles and then target them synthetically (33). In doing so, strongly enhanced Raman scattering signals of molecules in the vicinity of metal nanoparticles are being realized, which could provide substantial advancement in chemical-detection technology.

Photothermal Effect

The photothermal effect is another important feature of plasmonic nanoparticles. The exposure of plasmonic nanoparticles to light can convert the absorbed photons into phonons, leading to an increase in lattice temperature (86). The ultrafast laser-induced heating of hollow Au nanocages (94) and Ag nanocubes (95) has been fully investigated using time-resolved spectroscopy. In such experiments, a short pulse of light from a Ti:sapphire laser is split into pump and probe beams. The pump laser perturbs the absorption of the nanoparticles and causes the lattice temperature to increase. The transient change in absorption caused by the pump laser is then monitored using the probe laser. Analysis of the transient absorption trace provides information about the lattice temperature achieved, as well as the dynamics of heat dissipation. **Figure 13** shows the results obtained for 86-nm Ag nanocubes with a probe wavelength of 520 nm (95). Although calculations predict that the dominant mode excited should be the breathing mode of the cube, two vibrational modes were revealed in these experiments, with the high-frequency modulation assigned to the breathing mode and the low-frequency modulation to inhomogeneous heating.

Photothermal effect: a phenomenon that causes heating when a plasmonic particle is irradiated with an electromagnetic wave

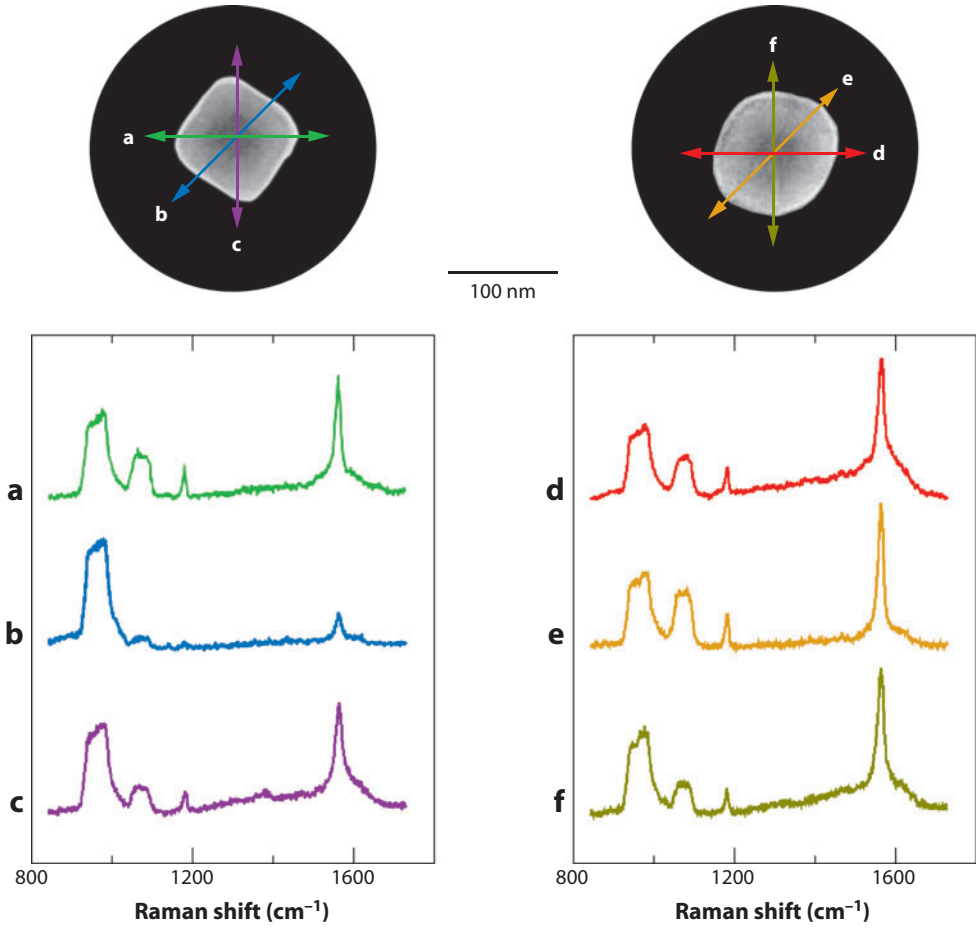

Figure 12

The normalized surface-enhanced Raman scattering spectra of 1,4-benzenedithiol adsorbed on an Ag nanocube with sharp corners (*left panel*, *a–c*) and a highly truncated Ag nanocube (*right panel*, *d–f*), at various angles relative to the polarization of the excitation laser. Each scanning electron micrograph shows the nanocube used, and the arrows indicate the polarization directions of incident laser. The scale bar applies to both images. The broad peak at 900–1000 cm^{-1} from the underlying Si substrate was used as the reference for normalization. Figure reproduced with permission from Reference 93. Copyright 2007 American Chemical Society.

A study on ultrafast laser-induced heating of Au nanocages has shown that extremely high lattice temperatures can be reached without reshaping the nanocages (94). This understanding of how electrons and phonons exchange energy with each other and with their environment was extended through similar experimental and theoretical studies to single-crystal Ag nanocubes (95). The information regarding the dynamics of energy relaxation following optical excitation of plasmonic nanoparticles is providing critical insight into the photothermal response of metal nanoparticles and could guide the design of new nanoparticles with improved photothermal response. Such materials are being considered as cancer-therapy agents, in which light-induced heating is targeted to destroy cancer cells, and solar-energy converters for efficient water heating.

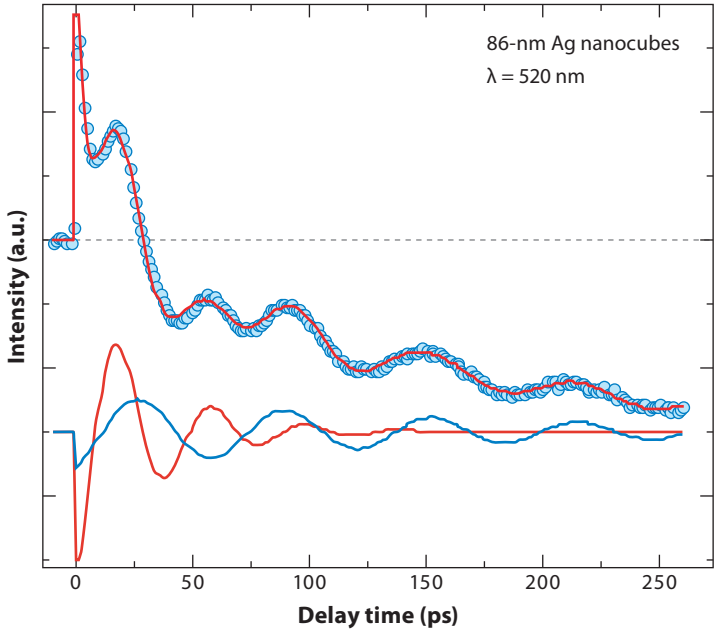

Figure 13

Pump-probe study of Ag nanocubes suspended in water. The representative transient absorption spectrum was recorded at a wavelength of 520 nm from 86-nm nanocubes. The solid line shows a fit to the data using two cosine terms and exponential decays to describe electron-phonon coupling and heat dissipation. The two cosine components extracted from the fit are shown below the experimental trace. Figure reproduced with permission from Reference 95. Copyright 2007 American Institute of Physics.

CONCLUSIONS

Plasmonic nanoparticles are of great interest because of their applications in photonics, optical sensing and imaging, SERS, and photothermal therapy. All these applications are enabled by the fascinating LSPR features of metal nanoparticles, a phenomenon that can be understood conceptually as the oscillation of free electrons in phase with incident light. As charge separation (surface polarization) is the main restoring force for oscillation, any morphological change to plasmonic nanoparticles will cause a spectral shift. Therefore, the shape-controlled chemical synthesis of plasmonic nanoparticles enables investigations of their LSPR and relevant applications systematically. By combining experimental study with theoretical calculations (based on Mie theory or DDA) of resonance responses for various nanoparticles, our knowledge on the relationship between the shape of a nanostructure and its optical properties continues to expand.

The precise control over the shape and size of plasmonic nanoparticles is not an easy task. Studies on the shape-controlled synthesis of Ag and Pd nanoparticles, as highlighted in this review, have shown that both the crystallinity of initial seeds produced and the growth rates of different crystallographic facets are pivotal to the shape of the resultant nanoparticles. Through manipulation of the reduction rates using kinetic control and oxidative etching, the distribution of seeds with different crystallinity can be altered to favor the growth of certain shapes exclusively. Although not elaborated on in this article, the capping agents selected for a given synthesis are also critical to shape control. By manipulating the growth rates of crystal facets using different

capping agents, new particles with desired morphologies and sizes may be accessed. Chemical synthetic methods are still in a rudimentary stage of development, although great progress has been made over the past decade. Molecular-level understanding on the formation of nuclei, seeds, and particles and their interactions with solvent and capping agents in solution would fundamentally impact theories of nanocrystal growth and expedite the development of syntheses for new shapes in high yields.

SUMMARY POINTS

1. LSPR describes the interaction between a plasmonic nanoparticle and electromagnetic wave irradiation. A change in the shape of the nanoparticle can alter its pattern of surface polarization and thus the LSPR significantly. This shape effect of LSPR can be used to tailor the spectral response of a particle through shape-controlled synthesis.
2. DDA calculation is a powerful numerical approach to obtain the light scattering and absorption of a metal particle with any arbitrary shape. Based on the DDA prediction for Ag nanoparticles, the trend for the change in LSPR with the shape of metal nanoparticles has been obtained. This trend can be used as the design rules for the preparation of nanoparticles with tunable LSPR.
3. Oxidative etching and kinetic control have proven in polyol synthesis to effectively generate nanoparticles with desirable shapes and optical spectra. Through oxidative etching, the defects in the growth seeds can be selectively etched, and only seeds with certain internal structures survive. Kinetically controlled reduction, conversely, can alter the reduction rate of the reaction and introduce stacking faults into the particles. Together, oxidative etching and kinetic control provide great flexibility in controlling the synthesis of Ag and Pd nanoparticles with various shapes such as cubes, bars, rods, bipyramids, and triangular and hexagonal plates. The spectral responses recorded from those nanostructures are consistent with the DDA predictions.
4. LSPR can create intense local electric fields within a few nanometers of a particle's surface. This near-field effect can improve Raman scattering cross sections of molecules adsorbed on the surface. Sharp corners on the surface of a nanoparticle tend to provide greater localized electric-field enhancement, and therefore the SERS EF, than rounded ones. Thus, controlling the shape of plasmonic nanoparticles plays an important role in maximizing the SERS EF. Noble-metal nanoparticles with well-controlled shapes and sizes serve as an ideal system to probe more thoroughly the underlying principles of SERS on metal structures.
5. Plasmonic nanoparticles can convert the energy absorbed from light into heat—a process called photothermal effect. Time-resolved spectroscopy has been employed to study the laser-induced heating of Ag nanocubes, and some insightful understanding on the photothermal response of metal nanoparticles has been obtained.

DISCLOSURE STATEMENT

The authors are not aware of any biases that might be perceived as affecting the objectivity of this review.

ACKNOWLEDGMENTS

The work described in this review was supported in part by research grants from the NSF (DMR, 0804088 and 0451788), ACS (PRF-44353-AC10), ONR (N-00014-01-1-0976); a DARPA-DURINT subcontract from Harvard University; and a 2006 Director's Pioneer Award from NIH (1DPOD000798). Y.X. was a Camille Dreyfus Teacher Scholar, an Alfred P. Sloan Research Fellow, and a David and Lucile Packard Fellow in Science and Engineering.

LITERATURE CITED

1. Xia Y, Halas NJ. 2005. Shape-controlled synthesis and surface plasmonic properties of metallic nanoparticles. *MRS Bull.* 30:338–44
2. Campbell DJ, Xia Y. 2007. Plasmons: Why should we care? *J. Chem. Educ.* 84:91–96
3. Ashcroft NW, Mermin ND. 1976. *Solid State Physics.* New York: Rinehart. 848 pp.
4. Brockman JM, Nelson BP, Corn RM. 2000. Surface plasmon resonance imaging measurements of ultrathin organic films. *Annu. Rev. Phys. Chem.* 51:41–63
5. Nath N, Chilkoti A. 2002. A colorimetric gold nanoparticle sensor to interrogate biomolecular interactions in real time on a surface. *Anal. Chem.* 74:504–9
6. Sun Y, Xia Y. 2002. Increased sensitivity of surface plasmon resonance of gold nanoshells compared to that of gold solid colloids in response to environmental changes. *Anal. Chem.* 74:5297–305
7. Thanh NTK, Rosenzweig Z. 2002. Development of an aggregation-based immunoassay for antiprotein A using gold nanoparticles. *Anal. Chem.* 74:1624–28
8. Fleischmann M, Hendra PJ, McQuillan AJ. 1974. Raman spectra of pyridine adsorbed at a silver electrode. *Chem. Phys. Lett.* 26:163–66
9. **Jeanmaire DL, Van Duyne RP. 1977. Surface Raman spectroelectrochemistry. Part I. Heterocyclic, aromatic, and aliphatic amines adsorbed on the anodized silver electrode. *J. Electroanal. Chem. Interfacial Electrochem.* 84:1–20**
10. Haynes CL, McFarland AD, Van Duyne RP. 2005. Surface-enhanced Raman spectroscopy. *Anal. Chem.* 77:A338–46
11. Maier SA, Kik PG, Atwater HA, Meltzer S, Harel E, et al. 2003. Local detection of electromagnetic energy transport below the diffraction limit in metal nanoparticle plasmon waveguides. *Nat. Mater.* 2:229–32
12. **Faraday M. 1857. Experimental relations of gold and other metals to light. *Philos. Trans. R. Soc. Lond.* 147:145–81**
13. Yguerabide J, Yguerabide EE. 1998. Light-scattering submicroscopic particles as highly fluorescent analogs and their use as tracer labels in clinical and biological applications, I. Theory. *Anal. Biochem.* 262:137–56
14. Mie G. 1908. Contributions to the optics of turbid media, especially colloidal metal solutions. *Anal. Phys.* 25:377–445
15. **Draine BT, Flatau PJ. 1994. Discrete-dipole approximation for scattering calculations. *J. Opt. Soc. Am.* 11:1491–99**
16. Yang WH, Schatz GC, Van Duyne RP. 1995. Discrete dipole approximation for calculating extinction and Raman intensities for small particles with arbitrary shapes. *J. Chem. Phys.* 103:869–75
17. **Wiley BJ, Im SH, Li Z-Y, McLellan J, Siekkinen A, Xia Y. 2006. Maneuvering the surface plasmon resonance of silver nanoparticles through shape-controlled synthesis. *J. Phys. Chem. B* 110:15666–75**
18. Kreibig U, Vollmer M. 1995. *Optical Properties of Metal Clusters.* New York: Springer. 532 pp.
19. Fuchs R. 1975. Theory of the optical properties of ionic crystal cubes. *Phys. Rev. B* 11:1732–40
20. Haes AJ, Haynes CL, McFarland AD, Schatz GC, Van Duyne RP, Zou SL. 2005. Plasmonic materials for surface-enhanced sensing and spectroscopy. *MRS Bull.* 30:368–75
21. Kottmann JP, Martin OJF, Smith DR, Schultz S. 2001. Plasmon resonances of silver nanowires with a nonregular cross section. *Phys. Rev. B* 64:235402
22. Aizpurua J, Bryant GW, Richter LJ, de Abajo FJG, Kelley BK, Mallouk T. 2005. Optical properties of coupled metallic nanorods for field-enhanced spectroscopy. *Phys. Rev. B* 71:235420

9. First paper proposing a mechanism for SERS.

12. First report of chemical synthesis of noble-metal plasmonic nanoparticles.

15. Detailed description of DDA calculation for the light scattering of particles.

17. Feature article describing the shape-controlled synthesis of Ag nanoparticles (see also References 25 & 33).

23. Kelly KL, Coronado E, Zhao LL, Schatz GC. 2003. The optical properties of metal nanoparticles: the influence of size, shape, and dielectric environment. *J. Phys. Chem. B* 107:668–77
24. Wiley BJ, Chen Y, McLellan JM, Xiong Y, Li Z-Y, et al. 2007. Synthesis and optical properties of silver nanobars and nanorice. *Nano Lett.* 7:1032–36
25. Wiley B, Sun Y, Xia Y. 2007. Synthesis of silver nanoparticles with controlled shapes and properties. *Acc. Chem. Res.* 40:1067–76
26. Wulff G. 1901. On the question of the rate of growth and dissolution of crystal surfaces. *Z. Kristallogr. Miner.* 34:449–530
27. Pimpinelli A, Villain J. 1998. *Physics of Crystal Growth*. Cambridge, UK: Cambridge Univ. Press. 408 pp.
28. Marks LD. 1994. Experimental studies of small-particle structures. *Rep. Prog. Phys.* 57:603–49
29. Venables JA. 2000. *Introduction to Surface and Thin Film Processes*. Cambridge, UK: Cambridge Univ. Press. 392 pp.
30. Komarneni S, Li DS, Newalkar B, Katsuki H, Bhalla AS. 2002. Microwave-polyol process for Pt and Ag nanoparticles. *Langmuir* 18:5959–62
31. Sun Y, Xia Y. 2002. Large-scale synthesis of uniform silver nanowires through a soft, self-seeding, polyol process. *Adv. Mater.* 14:833–37
32. Wiley B, Herricks T, Sun Y, Xia Y. 2004. Polyol synthesis of silver nanoparticles: use of chloride and oxygen to promote the formation of single-crystal, truncated cubes and tetrahedrons. *Nano Lett.* 4:1733–39
33. Wiley B, Sun Y, Mayers B, Xia Y. 2005. Shape-controlled synthesis of metal nanoparticles: the case of silver. *Chem. Eur. J.* 11:454–63
34. Silvert PY, Herrera-Urbina R, Duvauchelle N, Vijayakrishnan V, Elhsissen KT. 1996. Preparation of colloidal silver dispersions by the polyol process. 1. Synthesis and characterization. *J. Mater. Chem.* 6:573–77
35. Feldmann C. 2003. Polyol-mediated synthesis of nanoscale functional materials. *Adv. Funct. Mater.* 13:101–7
36. Fievet F, Fievet-Vincent F, Lagier JP, Dumont B, Figlarz M. 1993. Controlled nucleation and growth of micrometer-size copper particles prepared by the polyol process. *J. Mater. Chem.* 3:627–32
37. Wang Y, Xia Y. 2004. Bottom-up and top-down approaches to the synthesis of monodispersed spherical colloids of low melting-point metals. *Nano Lett.* 4:2047–50
38. Bonet F, Delmas V, Grugeon S, Urbina RH, Silvert PY, Tekaia-Elhsissen K. 1999. Synthesis of monodisperse Au, Pt, Pd, Ru and Ir nanoparticles in ethylene glycol. *Nanostruct. Mater.* 11:1277–84
39. Xiong Y, Xia Y. 2007. Shape-controlled synthesis of metal nanoparticles: the case of palladium. *Adv. Mater.* 19:3385–91
40. Wang ZL. 2000. Transmission electron microscopy of shape-controlled nanocrystals and their assemblies. *J. Phys. Chem. B* 104:1153–75
41. Smith DJ, Petford-Long AK, Wallenberg LR, Bovin JO. 1986. Dynamic atomic-level rearrangements in small gold particles. *Science* 233:872–75
42. Lofton C, Sigmund W. 2005. Mechanisms controlling crystal habits of gold and silver colloids. *Adv. Funct. Mater.* 15:1197–208
43. Wiley B, Sun Y, Chen J, Cang H, Li Z-Y, et al. 2005. Shape-controlled synthesis of silver and gold nanoparticles. *MRS Bull.* 30:356–61
44. Im SH, Lee YT, Wiley B, Xia Y. 2005. Large-scale synthesis of silver nanocubes: the role of HCl in promoting cube perfection and monodispersity. *Angew. Chem. Int. Ed. Engl.* 44:2154–57
45. Xiong Y, Chen J, Wiley B, Xia Y. 2005. Understanding the role of oxidative etching in the polyol synthesis of Pd nanoparticles with uniform shape and size. *J. Am. Chem. Soc.* 127:7332–33
46. Xiong Y, Chen J, Wiley B, Xia Y, Yin Y, Li Z-Y. 2005. Size-dependence of surface plasmon resonance and oxidation for Pd nanocubes synthesized via a seed etching process. *Nano Lett.* 5:1237–42
47. Chen J, Herricks T, Xia Y. 2005. Polyol synthesis of platinum nanoparticles: control of morphology through the manipulation of reduction kinetics. *Angew. Chem. Int. Ed. Engl.* 44:2589–92
48. Zettsu N, McLellan JM, Wiley B, Yin Y, Li Z-Y, Xia Y. 2006. Synthesis, stability, and surface plasmonic properties of rhodium multipods, and their use as substrates for surface-enhanced Raman scattering. *Angew. Chem. Int. Ed. Engl.* 45:1288–92

39. Recent article summarizing the shape-controlled synthesis of Pd nanostructures.

49. Wiley BJ, Xiong Y, Li Z-Y, Yin Y, Xia Y. 2006. Right bipyramids of silver: a new shape derived from single twinned seeds. *Nano Lett.* 6:765–68
50. Xiong Y, Cai H, Wiley BJ, Wang J, Kim MJ, Xia Y. 2007. Synthesis and mechanistic study of palladium nanobars and nanorods. *J. Am. Chem. Soc.* 129:3665–75
51. Murphy CJ, Gole AM, Hunyadi SE, Orendorff CJ. 2006. One-dimensional colloidal gold and silver nanoparticles. *Inorg. Chem.* 45:7544–54
52. McLellan JM, Siekkinen A, Chen J, Xia Y. 2006. Comparison of the surface-enhanced Raman scattering on sharp and truncated silver nanocubes. *Chem. Phys. Lett.* 427:122–26
53. Mock JJ, Barbic M, Smith DR, Schultz DA, Schultz S. 2002. Shape effects in plasmon resonance of individual colloidal silver nanoparticles. *J. Chem. Phys.* 116:6755–59
54. Yguerabide J, Yguerabide EE. 1998. Light-scattering submicroscopic particles as highly fluorescent analogs and their use as tracer labels in clinical and biological applications, II. Experimental characterization. *Anal. Biochem.* 262:157–76
55. Arya K. 2006. Scattering T-matrix theory in wave-vector space for surface-enhanced Raman scattering in clusters of nanoscale spherical metal particles. *Phys. Rev. B* 74:195438
56. Orendorff CJ, Gearheart L, Jana NR, Murphy CJ. 2006. Aspect ratio dependence on surface enhanced Raman scattering using silver and gold nanorod substrates. *Phys. Chem. Chem. Phys.* 8:165–70
57. Jana NR, Gearheart L, Murphy CJ. 2001. Wet chemical synthesis of high aspect ratio cylindrical gold nanorods. *J. Phys. Chem. B* 105:4065–67
58. Murphy CJ, Jana NR. 2002. Controlling the aspect ratio of inorganic nanorods and nanowires. *Adv. Mater.* 14:80–82
59. Nikoobakht B, El-Sayed MA. 2003. Preparation and growth mechanism of gold nanorods (NRs) using seed-mediated growth method. *Chem. Mater.* 15:1957–62
60. Chang SS, Shih CW, Chen CD, Lai WC, Wang CRC. 1999. The shape transition of gold nanorods. *Langmuir* 15:701–9
61. Kim F, Song JH, Yang PD. 2002. Photochemical synthesis of gold nanorods. *J. Am. Chem. Soc.* 124:14316–17
62. Pastoriza-Santos I, Liz-Marzan LM. 2002. Synthesis of silver nanoprisms in DMF. *Nano Lett.* 2:903–5
63. Chen S, Carroll DL. 2002. Synthesis and characterization of truncated triangular silver nanoplates. *Nano Lett.* 2:1003–7
64. Chen S, Fan ZY, Carroll DL. 2002. Silver nanodisks: synthesis, characterization, and self-assembly. *J. Phys. Chem. B* 106:10777–81
65. Yener DO, Sindel J, Randall CA, Adair JH. 2002. Synthesis of nanosized silver platelets in octylamine-water bilayer systems. *Langmuir* 18:8692–99
66. Maillard M, Giorgio S, Pileni MP. 2002. Silver nanodisks. *Adv. Mater.* 14:1084–86
67. Jin R, Cao Y, Mirkin CA, Kelly KL, Schatz GC, Zheng J. 2001. Photoinduced conversion of silver nanospheres to nanoprisms. *Science* 294:1901–3
68. Jin R, Cao Y, Hao E, Metraux GS, Schatz GC, Mirkin CA. 2003. Controlling anisotropic nanoparticle growth through plasmon excitation. *Nature* 425:487–90
69. Sun Y, Xia Y. 2003. Triangular nanoplates of silver: synthesis, characterization, and use as sacrificial templates for generating triangular nanorings of gold. *Adv. Mater.* 15:695–99
70. Sun Y, Mayers B, Xia Y. 2003. Transformation of silver nanospheres into nanobelts and triangular nanoplates through a thermal process. *Nano Lett.* 3:675–79
71. Washio I, Xiong Y, Yin Y, Xia Y. 2006. Reduction by the end groups of poly(vinyl pyrrolidone): a new and versatile route to the kinetically controlled synthesis of Ag triangular nanoplates. *Adv. Mater.* 18:1745–49
72. Sun Y, Xia Y. 2002. Shape-controlled synthesis of gold and silver nanoparticles. *Science* 298:2176–79
73. Xiong Y, Washio I, Chen J, Cai H, Li Z-Y, Xia Y. 2006. Poly(vinyl pyrrolidone): a dual functional reductant and stabilizer for the facile synthesis of noble metal nanoplates in aqueous solutions. *Langmuir* 22:8563–70
74. Xiong Y, Washio I, Chen J, Sadilek M, Xia Y. 2007. Trimeric clusters of silver in aqueous $AgNO_3$ solutions and their role as nuclei in forming triangular nanoplates of silver. *Angew. Chem. Int. Ed. Engl.* 46:4917–21

72. First paper describing the preparation of Ag nanocubes as sacrificial templates in a galvanic replacement reaction to form hollow nanoboxes.

74. Report relating the existence of trimeric Ag clusters and the formation of Ag triangular plates in solution-phase synthesis.

75. Sosa IO, Noguez C, Barrera RG. 2003. Optical properties of metal nanoparticles with arbitrary shapes. *J. Phys. Chem. B* 107:6269–75
76. Xiong Y, McLellan JM, Chen J, Yin Y, Li Z-Y, Xia Y. 2005. Kinetically controlled synthesis of triangular and hexagonal nanoplates of palladium and their SPR/SERS properties. *J. Am. Chem. Soc.* 127:17118–27
77. Xiong Y, McLellan JM, Yin Y, Xia Y. 2007. Synthesis of palladium icosahedra with twinned structure by blocking oxidative etching with citric acid or citrate ions. *Angew. Chem. Int. Ed. Engl.* 46:790–94
78. Xiong Y, Cai H, Yin Y, Xia Y. 2007. Synthesis and characterization of fivefold twinned nanorods and right bipyramids of palladium. *Chem. Phys. Lett.* 440:273–78
79. Zou S, Weaver MJ. 1996. Potential-dependent metal-adsorbate stretching frequencies for carbon monoxide on transition-metal electrodes: chemical bonding versus electrostatic field effects. *J. Phys. Chem.* 100:4237–42
80. Tian Z, Ren B, Wu D. 2002. Surface-enhanced Raman scattering: from noble to transition metals and from rough surfaces to ordered nanoparticles. *J. Phys. Chem. B* 106:9463–83
81. Gomez R, Perez JM, Solla-Gullon J, Montiel V, Aldaz A. 2004. In situ surface enhanced Raman spectroscopy on electrodes with platinum and palladium nanoparticle ensembles. *J. Phys. Chem. B* 108:9943–49
82. Tobiska P, Hugon O, Trouillet A, Gagnaire H. 2001. An integrated optic hydrogen sensor based on SPR on palladium. *Sens. Actuators B* 74:168–72
83. Sun Y, Tao Z, Chen J, Herricks T, Xia Y. 2004. Ag nanowires coated with Ag/Pd alloy sheaths and their use as substrates for reversible absorption and desorption of hydrogen. *J. Am. Chem. Soc.* 126:5940–41
84. Willets KA, Van Duyne RP. 2007. Localized surface plasmon resonance spectroscopy and sensing. *Annu. Rev. Phys. Chem.* 58:267–97
85. Liao HW, Nehl CL, Hafner JH. 2006. Biomedical applications of plasmon resonant metal nanoparticles. *Nanomedicine* 1:201–8
86. Hu M, Chen JY, Li ZY, Au L, Hartland GV, et al. 2006. Gold nanoparticles: engineering their plasmonic properties for biomedical applications. *Chem. Soc. Rev.* 35:1084–94
87. Banholzer MJ, Millstone JE, Qin L, Mirkin CA. 2008. Rationally designed nanoparticles for surface-enhanced Raman spectroscopy. *Chem. Soc. Rev.* 37:885–97
88. Jensen L, Aikens CM, Schatz GC. 2008. Electronic structure methods for studying surface-enhanced Raman scattering. *Chem. Soc. Rev.* 37:1061–73
89. Hao E, Schatz GC. 2004. Electromagnetic fields around silver nanoparticles and dimers. *J. Chem. Phys.* 120:357–66
90. Moskovits M. 2005. Surface-enhanced Raman spectroscopy: a brief retrospective. *J. Raman Spectrosc.* 36:485–96
91. Zeman EJ, Schatz GC. 1987. An accurate electromagnetic theory study of surface enhancement factors for silver, gold, copper, lithium, sodium, aluminum, gallium, indium, zinc, and cadmium. *J. Phys. Chem.* 91:634–43
92. Sherry LJ, Chang SH, Schatz GC, Van Duyne RP, Wiley BJ, Xia Y. 2005. Localized surface plasmon resonance spectroscopy of single silver nanocubes. *Nano Lett.* 5:2034–38
93. McLellan JM, Li Z-Y, Siekkinen AR, Xia Y. 2007. The SERS activity of a supported Ag nanocube strongly depends on its orientation relative to laser polarization. *Nano Lett.* 7:1013–17
94. Hu M, Petrova H, Chen J, McLellan JM, Siekkinen AR, et al. 2006. Ultrafast laser studies of the photothermal properties of gold nanocages. *J. Phys. Chem. B* 110:1520–24
95. Petrova H, Lin C, de Liejer S, Hu M, McLellan JM, et al. 2007. Time-resolved spectroscopy of silver nanocubes: observation and assignment of coherently excited vibrational modes. *J. Chem. Phys.* 126:094709

92. First observation of the dependence of a supporting substrate on LSPR of a single Ag nanocube.

93. First study on the variation of SERS intensity with orientations of an Ag nanocube with respect to the polarization of an excitation laser.

Annual Review of
Physical Chemistry

Volume 60, 2009

Contents

Indexes

Errata

An online log of corrections to *Annual Review of Physical Chemistry* articles may be found at http://physchem.annualreviews.org/errata.shtml